Inverse-velocity transformation wall model for reacting turbulent hypersonic boundary layers

By M. Cogo†, C. T. Williams, K. P. Griffin ‡, F. Picano¶† AND P. Moin

1. Motivation and objectives

The design of supersonic and hypersonic systems is predicated upon the ability to accurately predict aerothermodynamics loads acting on the surface of the vehicle (Bertin & Cummings 2006; Candler 2019). At high Mach numbers, the combined presence of shock waves, turbulence, and thermochemical processes affects significantly the performance and structural integrity of the aircraft and its propulsion system (Park 1990; Anderson 2006; Urzay 2018). The ability to resolve physical and chemical processes with such heterogeneous spatial and temporal scales, especially near the wall, requires such massive computational resources and suitable numerical tools that only very recently has direct numerical simulation (DNS) become feasible for flat plate boundary layers (Di Renzo & Urzay 2021; Passiatore *et al.* 2022; Williams *et al.* 2023). In this regard, the development of wall models is essential to mitigate the computational effort for canonical flows and enable simulation of more complex flow configurations of scientific interest.

One of the most employed class of wall models, the equilibrium wall model (EWM), can be derived from the Reynolds-averaged formulation of the Navier–Stokes equations assuming a constant stress layer. In the past decade, significant improvements have been made to provide a suitable formulation of the classical EWM for relatively high Mach numbers and intense wall cooling (Kawai & Larsson 2010; Bose & Park 2018; Yang *et al.* 2018; Iyer & Malik 2019). More recently, Griffin *et al.* (2023) proposed a near-wall model based on an inverse velocity transformation of Griffin *et al.* (2021) and an algebraic temperature–velocity relation (Zhang *et al.* 2014). Their study showed improved results compared to the classical EWM, especially for highly compressible flows with large wall heat fluxes, with the added advantage of needing to solve only one ordinary differential equation (ODE) instead of two.

Notwithstanding the recent developments in high-speed boundary-layer modeling, making the effort to account for high temperature effects in chemically reacting multicomponent mixtures is still rare, owing to the added modeling complexity and lack of availability of reference data. Recently, Muto *et al.* (2019) proposed an extension of the EWM to multicomponent mixtures in chemical equilibrium. Efforts to account for differential diffusion and finite-rate chemistry were later made by Di Renzo & Urzay (2019), who conducted an *a priori* study in supersonic channel flows. In particular, this study compared two different mixing length models to estimate the eddy viscosity, finding that the semilocal formulation of the Van Driest damping factor provided the best results. However, large discrepancies with reference data were still present in the prediction of oxygen molar fraction profiles and were attributed to modeling errors of the chemical source term.

The present study builds on prior work by taking advantage of the novel framework

† CISAS "Giuseppe Colombo", University of Padova, Italy
‡ National Renewable Energy Laboratory
¶ Department of Industrial Engineering, University of Padova, Italy

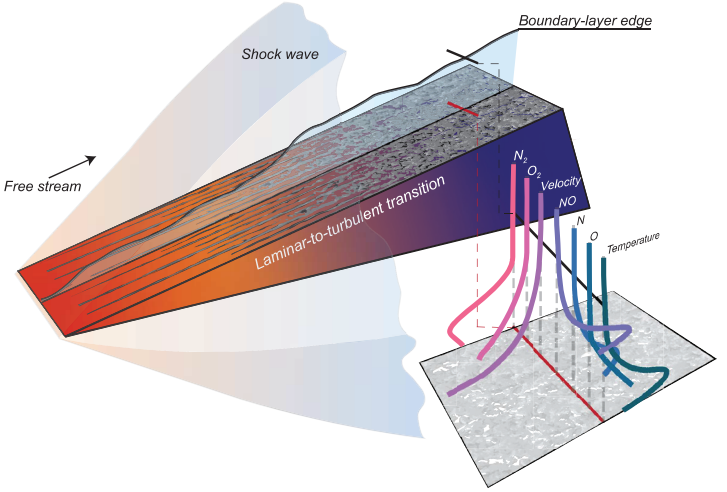

FIGURE 1. Schematic of a hypersonic flow configuration over a wedge and the underlying variation of flow properties in the turbulent region.

proposed by Griffin *et al.* (2023) (hereafter referred to as the GFM) as a baseline. The model is progressively extended to multicomponent reacting mixtures, accounting for differential diffusion and finite-rate chemistry in a similar fashion to Di Renzo & Urzay (2019) and Di Renzo *et al.* (2020). The accuracy of the present approach, as well the prior model of Di Renzo & Urzay (2019), is assessed in an *a priori* sense for the first time in a turbulent reacting boundary layer, using the boundary-layer data of Williams *et al.* (2023). Five species are included in the present analysis, i.e., $N_s = 5$, namely N_2, O_2, NO, N and O, a neutral mixture most representative of dissociation/recombination phenomena for temperatures below 6000 K. A schematic of a flow over a wedge representative of the described configuration is presented in Figure 1.

The brief is organized as follows: In Section 2, the wall-model equations and the computational framework are presented. In Section 3, the *a priori* results of the proposed model are described and compared to the extended EWM. Finally, in Section 4, some conclusions are offered.

2. Wall-model equations

The present model aims to predict the average wall stress, heat flux, and composition of a wall-bounded flow that obeys the compressible Navier–Stokes equations subject to species transport in a chemically reacting mixture of ideal gases. In the classical formulation, the conserved variables consist of the partial densities $\rho_i = \rho Y_i$ of the i-th species in the mixture; the three components of momentum per unit volume ρu, ρv, and ρw; and the specific stagnation internal energy $e_0 = e + |\mathbf{u}|^2/2$, with e being the specific internal energy of the mixture and $\mathbf{u}$, the velocity vector. The reader can find a thorough description of the underlying conservation equations and thermochemistry in Williams *et al.* (2023).

In the context of wall modeling, a general formulation of the transport equations is based on the primitive variables $\tilde{u}$, $\tilde{T}$, and $\tilde{Y}_i$, from which the desired wall quantities and mixture properties can be derived. In section 2.1, a summary of the extended EWM proposed by Di Renzo & Urzay (2019) is given, and Sections 2.2 and 2.3 report the

present extension of the GFM. In particular, the former presents a first generalization of the original model to thermally perfect gases with frozen composition, while the latter includes the coupling with the equations of species partial density for reacting flows. Throughout this brief, the superscript $^+$ indicates a nondimensionalization by the friction velocity $u_\tau = \sqrt{\tau_w/\rho_w}$, the viscous length scale $\delta_\nu = \mu_w/(u_\tau \rho_w)$, ρ_w; and μ_w, where τ_w, ρ_w and μ_w are the shear stress, density, and dynamic viscosity evaluated at the wall, respectively.

2.1. *Equilibrium-wall-model equations for a reacting mixture*

The extended EWM for reacting flows of Di Renzo & Urzay (2019) is based on the Favre-averaged transport equations simplified with the constant stress layer assumption. The conservation equations for momentum, enthalpy, and species partial density read

$$\begin{aligned}
&\frac{d}{dy}\left[\left(\widetilde{\mu}+\mu_t\right)\frac{d\widetilde{u}}{dy}\right]=0,\\
&\frac{d}{dy}\left[\widetilde{u}\left(\widetilde{\mu}+\mu_t\right)\frac{d\widetilde{u}}{dy}+\widetilde{\lambda}\frac{d\widetilde{T}}{dy}+\frac{\mu_t}{Pr_t}\frac{d\widetilde{h}}{dy}-\sum_{i=1}^{N_s}\bar{\rho}_i\widetilde{V}_{y,i}\widetilde{h}_i\right]=0, \text{and}\\
&\frac{d}{dy}\left(-\bar{\rho}_i\widetilde{V}_i+\frac{\mu_t}{Sc_t}\frac{d\widetilde{Y}_i}{dy}\right)+\overline{\dot{w}}_i=0, \qquad \text{for } i=1,\ldots,N_s.
\end{aligned} \tag{2.1}$$

The reader can find in Di Renzo & Urzay (2019) the definition of mixture properties, wall-normal diffusion velocities $\widetilde{V}_i$, partial specific enthalpies $\tilde{h}_i$, and production rates $\overline{\dot{w}}_i$. Di Renzo & Urzay (2019) invoke the laminar closure for the transport of reaction rates, $\overline{\dot{w}_i} = f(\tilde{T}, \bar{\rho}, \tilde{Y}_i)$, which neglects the fluctuations of each variable and assumes a statistical independence between them. The turbulent Prandtl number Pr_t and the turbulent Schimdt number Sc_t were assumed equal to 0.9.

The eddy viscosity μ_t is computed with a mixing length model, which reads

$$\mu_t = k\bar{\rho}y\sqrt{\frac{\tau_w}{\bar{\rho}}}\left[1-exp\left(-\frac{y^*}{A^+}\right)\right]^2, \tag{2.2}$$

where $A^+ = 17$ and $k = 0.41$. This formulation employs the semilocal-scaled wall-normal coordinate $y^* = y/(\bar{\nu}/\sqrt{\tau_w/\bar{\rho}})$ in the Van Driest damping function, which has been shown to better account for compressibility effects compared to the classical version using y^+ (Yang & Lv 2018).

The set of ODEs of Eq. (2.1), the extended EWM, and the eddy viscosity model of Eq. (2.2), will be considered in this study for comparison.

2.2. *GFM equations for a thermally perfect frozen mixture*

The original formulation of the GFM, (Griffin *et al.* 2023), leverages the compressibility transformation of Griffin *et al.* (2021) and the temperature-velocity relation of Zhang *et al.* (2014) to build a framework which especially targets high-speed flows with strong heat transfer. The proposed model was formulated for calorically perfect gases and showed clear improvements from the classical EWM, better accounting for compressibility and wall-cooling effects, which are relevant for applications in the hypersonic regime. In this section, a preliminary extension of this model is proposed for thermally perfect mixtures with constant composition, meaning that the chemical state is considered frozen (i.e., chemical timescales are much larger than fluid dynamics timescales), while the variation of the specific heat with temperature $c_p = f(T)$ is taken into account.

Following the study of Griffin *et al.* (2023), the inverse velocity transformation equation is first considered, which reads as

$$\frac{d\tilde{U}^+}{dy^*} = \left(\frac{1}{\bar{\mu}^+ S_t^+} - \frac{1}{\bar{\mu}^+} + \sqrt{\bar{\rho}^+} \left(1 + \frac{1}{2\bar{\rho}^+} \frac{d\bar{\rho}^+}{dy^+} y^+ - \frac{1}{\bar{\mu}^+} \frac{d\bar{\mu}^+}{dy^+} y^+ \right) \right)^{-1}. \tag{2.3}$$

In this formulation, the incompressible mean strain rate $S_t^+ = dU^+/dy^+$ can be algebraically computed from the constant property version of the relation $dU/dy = \tau_w/(\mu + \mu_t)$, where μ_t is the eddy viscosity estimated with the classical mixing length model. It is important to note that the evalutation of μ_t is needed only to compute the incompressible mean strain rate, whereas the compressible counterpart is evaluated without assuming any model for the eddy viscosity, which will be relevant later in this section. In the original formulation, the velocity is coupled with the temperature by means of an algebraic law that assumes a quadratic relationship between the two quantities (Duan & Martin 2011; Zhang *et al.* 2014). The relation has been reformulated by Griffin *et al.* (2023) to be exactly consistent with the matching data rather than the edge data (i.e., $h = h_m$ if $U = U_m$, but $h \neq h_e$ when $U = U_e$) to obtain

$$\tilde{T} = \tilde{T}_w + sPr \left(\tilde{T}_r - \tilde{T}_w \right) \frac{\tilde{U}}{\tilde{U}_e} \left(1 - \frac{\tilde{U}}{\tilde{U}_m} \right) + \left(\frac{\tilde{U}}{\tilde{U}_m} \right)^2 \left(\tilde{T}_m - \tilde{T}_w \right), \tag{2.4}$$

where subscripts $_m$ and $_e$ indicate quantities computed at the matching location and at the edge of the boundary layer, respectively.

In a thermally perfect regime, the more general enthalpy–velocity relation is considered (Duan & Martin 2011), being consistent with the nonlinear relationship between temperature and enthalpy, which reads

$$\tilde{h} = \tilde{h}_w + s\,\mathrm{Pr} \left(\tilde{h}_r - \tilde{h}_w \right) \frac{\widetilde{U}}{\widetilde{U}_e} \left(1 - \frac{\widetilde{U}}{\widetilde{U}_e} \right) + \left(\frac{\widetilde{U}}{\widetilde{U}_m} \right)^2 \left(\tilde{h}_e - \tilde{h}_w \right), \tag{2.5}$$

where s is the Reynolds analogy factor, Pr is the Prandtl number, and $\tilde{h}_r = \tilde{h}_e + r\tilde{U}_e^2/2$ is the recovery enthalpy.

In this relation, the product $sPr = 0.82$ is assumed to be constant and equal to the fitted value of Zhang *et al.* (2014) (also supported by Cogo *et al.* (2023) for cold walls), while the recovery factor is taken as $r = 0.89$. A preliminary assessment of the accuracy of the enthalpy–velocity relation proposed in Eq. (2.5) is presented in Figure 2, which also reports the original temperature–velocity relation of Griffin *et al.* (2023). It is apparent that while the latter clearly deviates from the DNS profile, the former has a very good agreement especially at low speeds (near the wall). In light of similar findings from Passiatore *et al.* (2022), which considered a chemically and thermally out-of-equilibrium mixture, the enthalpy–velocity relationship seems to be relatively robust. Temperature is a nonlinear function of enthalpy and composition, and thus large variations in temperature are observed based on the composition/chemistry modeling.

2.3. *Extension of GFM equations for a reacting mixture*

This section further extends the formulation proposed in Section 2.2 to reacting mixtures, accounting for differential diffusion and finite-rate chemistry in a similar fashion to Di Renzo & Urzay (2019). In the present formulation, Eqs. (2.3)-(2.5) are coupled to the species partial density equations, yielding the following nonlinear system

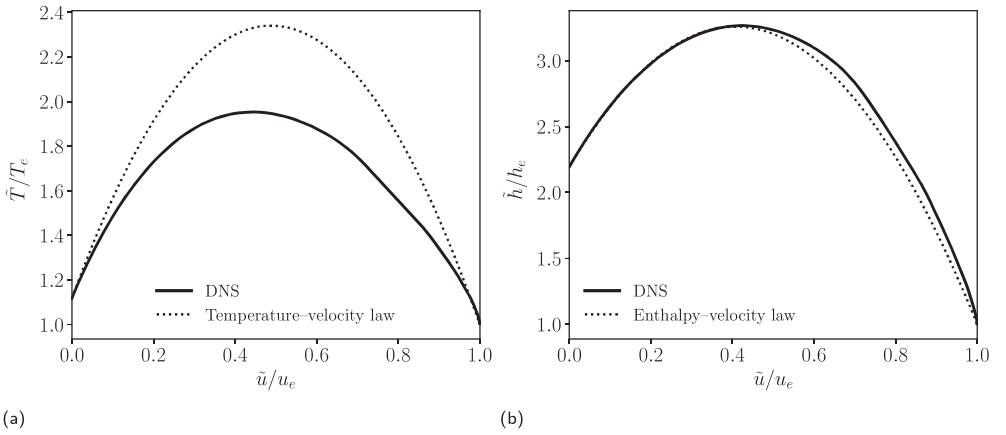

FIGURE 2. Comparison of the accuracy of algebraic laws for (a) temperature–velocity, Eq. (2.4), and (b) enthalpy–velocity, Eq. (2.5). DNS data from Williams *et al.* (2023).

$$\begin{aligned}
&\frac{d\tilde{U}^+}{dy^*} = \left(\frac{1}{\bar{\mu}^+ S_t^+} - \frac{1}{\bar{\mu}^+} + \sqrt{\bar{\rho}^+}\left(1 + \frac{1}{2\bar{\rho}^+}\frac{d\bar{\rho}^+}{dy^+}y^+ - \frac{1}{\bar{\mu}^+}\frac{d\bar{\mu}^+}{dy^+}y^+\right)\right)^{-1}, \\
&\tilde{h} = \tilde{h}_w + s\,\mathrm{Pr}\left(\tilde{h}_r - \tilde{h}_w\right)\frac{\widetilde{U}}{\widetilde{U}_e}\left(1 - \frac{\widetilde{U}}{\widetilde{U}_e}\right) + \left(\frac{\widetilde{U}}{\widetilde{U}_m}\right)^2\left(\tilde{h}_e - \tilde{h}_w\right), \text{and} \\
&\frac{d}{dy}\left(-\bar{\rho}_i\widetilde{V}_i + \frac{\mu_t}{Sc_t}\frac{d\widetilde{Y}_i}{dy}\right) + \overline{\dot{w}}_i = 0, \qquad \text{for } i = 1, \ldots, N_s
\end{aligned} \tag{2.6}$$

where Sc_t is assumed equal to 0.9 and laminar closure is employed to model the chemical reaction rate $\overline{\dot{w}}_i$ (refer to Section 2.1). A key difference from the prior work of Di Renzo & Urzay (2019) is that the eddy viscosity μ_t present in the species equation is not modeled with the semilocal formulation of the mixing length assumption of Eq. (2.2).

In fact, since the inverse velocity transformation, Eq. (2.3), relies only on the classical mixing length model for incompressible flows, the eddy viscosity can be directly computed from the compressible mean strain rate $d\tilde{U}^+/dy^*$ by assuming a constant stress layer as

$$\left.\frac{dU^+}{dy^*}\right|_{GFM}\frac{dy^*}{dy}u_\tau = \frac{\tau_w}{\mu + \mu_t}. \tag{2.7}$$

This approach directly couples the eddy viscosity model for a given compressible flow to the compressibility transformation under consideration, without having to define a compressible version of the mixing length model to account for the variability of the thermodynamical properties.

2.4. *Computational framework*

The proposed extension of the GFM consists of the nonlinear system described in Eq. (2.6), which can be numerically solved from the wall to an arbitrary matching location. In the present analysis, the performance of the model is evaluated in an *a priori* sense, meaning that the thermodynamic state and the streamwise velocity at the matching location are obtained from Favre-averaged DNS data, which are enforced as the outer

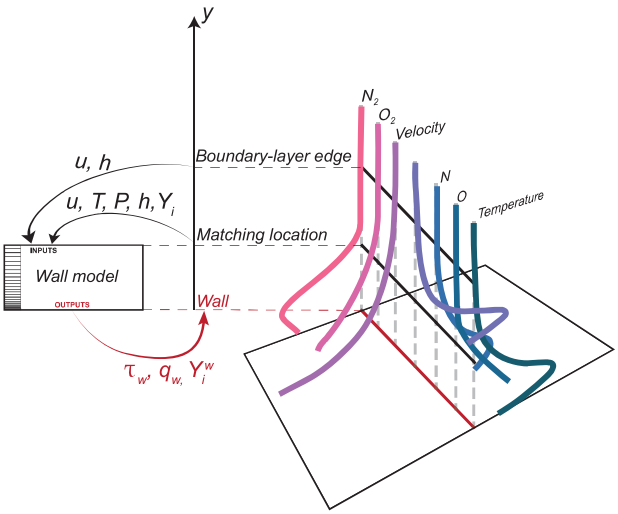

FIGURE 3. Schematic of a wall model implementation for high-speed turbulent boundary layers with variable composition.

boundary condition of the problem. At the wall, no-slip, isothermal and non-catalytic conditions are imposed. Finally, values for the streamwise velocity and enthalpy at the boundary-layer edge are required. A schematic of the wall model implementation is reported in Figure 3, which summarizes the inputs and outputs, as well as a qualitative representation of relevant wall-normal profiles.

The numerical solution of the system of equations is obtained following the approach of Di Renzo & Urzay (2019), which employed a multivariate Newton solver modified with a line-search algorithm. The equations are discretized on a stretched grid of 150 points using second-order finite differences; a tolerance of 10^{-12} is required to establish convergence. The performance of the extended EWM and GFMs is evaluated using two hypothetical matching locations at $y_m^+ = 15$ and 100. The former is selected near the wall where both models are expected to show a good agreement, while the latter lies in the log layer, $y/\delta_{99} \approx 0.1$, and is placed well beyond the mean temperature peak, a critical feature to reproduce for these type of flows. Here, δ_{99} indicates the local boundary-layer thickness at 99% of the mean streamwise velocity.

Finally, additional results obtained with frozen chemistry are included, meaning that transport equations for species are not carried and the composition is kept constant to the value imposed at the matching location. These results represent a measure of the influence that the coupling with mass fraction profiles has in the prediction of primary quantities of interest (i.e., velocity and temperature).

3. Results

The present study is based primarily on the reference DNS dataset of Williams *et al.* (2023), which consists of a reacting turbulent hypersonic boundary layer with an edge Mach number of $M_e = 7$ and edge temperature of $T_e = 2700$ K. The selected streamwise location is characterized by a friction Reynolds number of $Re_\tau \equiv \delta_{99}/\delta_\nu = 1161$. The intense thermochemical processes present in this database, and their strong interaction with turbulence, represent a challenging environment that is beneficial to the assessment

Case	$\epsilon_{\tau_w}(\%)$	$\epsilon_{q_w}(\%)$	$\epsilon_{Y^w_{N_2}}(\%)$	$\epsilon_{Y^w_O}(\%)$
EWM015	2.4	8.3	0.04	-0.03
GFM015	0.70	1.1	0.02	-0.05
EWM100	-8.8	-5.2	-0.42	-1.9
GFM100	-2.4	-1.2	-0.35	-1.4

TABLE 1. *A priori* modeling errors of wall shear stress τ_w, wall heat flux q_w, and major species mass fraction $Y^w_{N_2}$ and Y^w_O at the wall. Errors are reported for both the extended EWM and GFM at matching locations $y^+_m = 15$ and 100. DNS data from Williams *et al.* (2023).

of the model's accuracy. The reader is referred to Williams *et al.* (2023) for a detailed description of the computational setup and mean-flow statistics.

A first impression of the accuracy of the extended EWM and the extended GFM is given in Figure 4, which reports the inner-scaled velocity u^+ and rescaled temperature T/T_w profiles. Additionally, results obtained with frozen chemistry are included. Analyzing at Figure 4(a,c), it can be noted that all profiles matching at $y^+ = 15$ have a good agreement with reference data. Slight underprediction of the temperature profile is visible for the extended EWM. Quantitative errors in the prediction of the wall shear stress τ_w and wall heat flux q_w are reported in Table 1, where the extended GFM shows clear improvements. A general overview of profiles matching at $y^+ = 100$ shows a consistent improvement of the GFM in the predictions of both velocity and temperature profiles. In particular, compared to the EWM model, smaller deviations from DNS are present in the log-layer intercept of the velocity profile, Figure 4(b), and there is a reduced overestimation of the temperature peak, Figure 4(d). The loss of accuracy due to the frozen chemistry assumption is clearly visible in Figure 4(d), which still shows an improved accuracy of the GFM for these cases. In Figure 4(b), this aspect is less evident and frozen profiles seem to predict slightly better the log-layer intercept. This behavior is attributed to the cancellation of errors and corroborates the idea that velocity profiles are less sensitive to changes in composition in comparison to the temperature.

As discussed in Section 2, the evaluation of the compressible mean strain rate of Eq. (2.3) not only is relevant to derive the mean velocity profile but also can be leveraged to predict the eddy viscosity without relying on a compressible mixing length model. Figure 5 compares the proposed approach of Eq. (2.7) with the standard mixing length assumption with the semilocal formulation of Eq. (2.2) used in the extended EWM, showing an improved agreement with DNS data as the matching location is moved farther from the wall.

Figure 6 reports the profiles of enthalpy $\tilde{h}/h_{ref}$, Figure 6(a), and the five mass fractions $\tilde{Y}_i$, Figure 6(b-f). Here, it is worth recalling that enthalpy has a nonlinear dependence with temperature, and is also a function of the local composition. In Figure 6(a), the GFM shows an excellent prediction of the enthalpy profile compared with DNS data, while the EWM exhibits an overprediction in the buffer layer that culminates in the peak region. A considerable loss of accuracy is visible for frozen cases, especially near the wall. This

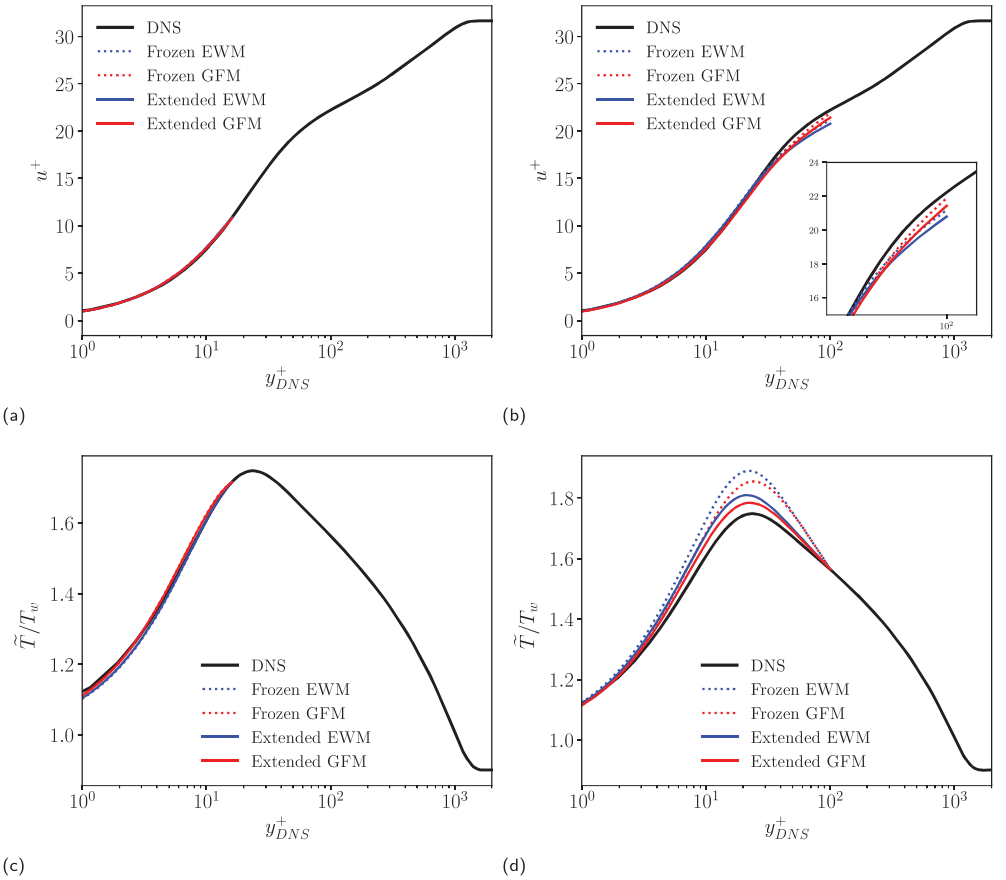

FIGURE 4. Favre-averaged profiles of (a,b) inner-scaled streamwise velocity u^+ and (c,d) rescaled temperature $\tilde{T}/T_w$ as function of the DNS y^+. The matching location corresponds to either (a,c) $y^+_{DNS} = 15$, or (b,d) $y^+_{DNS} = 100$. DNS data from Williams *et al.* (2023).

is expected because while DNS values of mass fractions are imposed at the matching location, the correct enthalpy at the wall cannot be retrieved by assuming a constant composition throughout the boundary layer. Figure 6(b-f) shows results on the prediction of mass fraction profiles, namely $\tilde{Y}_{N_2}$, $\tilde{Y}_{O_2}$, $\tilde{Y}_{NO}$, $\tilde{Y}_N$, and $\tilde{Y}_O$. A general overview of all profiles shows minimal differences between the EWM and the GFM, the former being slightly better in the prediction of $\tilde{Y}_N$ and the latter showing marginally improved results in all other compounds. However, both models show deviations from DNS data that result in under-/overpredictions of mass fractions at the wall as well as incorrect prediction of gradients at the matching location visible for certain compounds (e.g., see inset of Figure 6(e) for $\tilde{Y}_{NO}$). It is worth noting that both models progressively approach DNS data when the matching location is between the wall and the temperature peak (not shown). Modeling errors regarding the wall values of $\tilde{Y}_{N_2}$ and $\tilde{Y}_O$ are available in Table 1, as these are the most abundant species in the mixture, while the others species are close to zero at the wall. Although errors at the wall are relatively small, clear differences with DNS profiles can be noted in the predicted gradients at the matching location. The fact

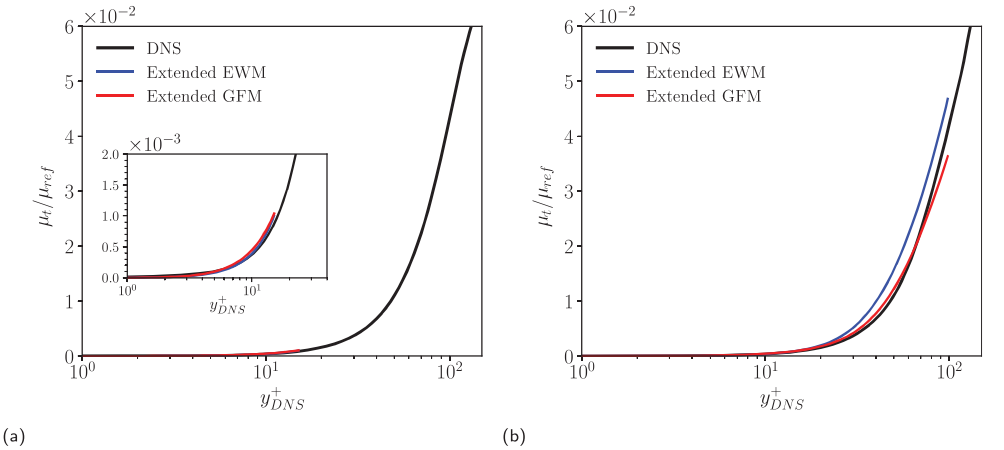

FIGURE 5. Comparison of the eddy viscosity μ_t profiles as function of y^+_{DNS} computed with the extended EWM (semilocal mixing length model) of Eq. (2.2) and the extended GFM of Eq. (2.7). DNS data refer to the theoretical value of the Boussinesq approximation $-\bar{\rho}\widetilde{u''v''}/(d\tilde{u}/dy)$. The matching locations correspond to (a) $y^+_{DNS} = 15$ and (b) $y^+_{DNS} = 100$. DNS data from Williams *et al.* (2023).

that this feature is shared by both models suggests that specific assumptions included in the Favre-averaged equations of species overshadow differences induced by their coupling with other quantities discussed above ($\tilde{u}$, $\tilde{T}$).

From the discussion of Williams *et al.* (2023), it is apparent that the laminar closure model for the chemical reaction rate $\overline{\dot{w}}_i$ has clear shortcomings that become progressively more drastic as the turbulence–chemistry interaction level increase. In particular, accurately accounting for correlated fluctuations in the temperature and partial density fields is fundamental for prediction of the mean chemical production rate throughout the boundary layer, which cannot be predicted only with averaged quantities.

In order to more objectively address the influence of this assumption on both models, Figure 7 shows the resulting profiles of enthalpy and mass fractions when the DNS profiles of chemical reaction rates are enforced in the solution, $\overline{\dot{w}}_i = f(y)|_{DNS}$. Here, it is visible how the extended GFM drastically improves the prediction of the correct gradient at the matching location for all species, which are in very good agreement with DNS data. This improvement is shared with the EWM only for certain compounds ($\tilde{Y}_{N_2}$, $\tilde{Y}_{NO}$), while for the other species the prediction is actually worse. For these compounds, it is expected that cancellation of errors could play a role because discrepancies with DNS were already small and other modeling assumptions may become relevant. At the wall, the extended GFM shows an excellent agreement with DNS data (see also Table 2), except for $\tilde{Y}_N$, which may be affected by other modeling errors. It should be noted that the improved behavior of the mass fractions profiles by including $\overline{\dot{w}}_i = f(y)|_{DNS}$ is not shared with the enthalpy profiles, nor velocity and temperature profiles, which shows almost identical results (not shown). This is also visible in the shear stress and heat flux predictions reported in Table 2, although it is important to note that errors were already relatively low.

Case	$\epsilon_{\tau_w}(\%)$	$\epsilon_{q_w}(\%)$	$\epsilon_{Y^w_{N_2}}(\%)$	$\epsilon_{Y^w_O}(\%)$
EWM100*	-8.7	-5.4	-0.12	-2.5
GFM100*	-2.4	-1.0	-0.11	0.11

TABLE 2. *A priori* modeling errors of wall shear stress τ_w, wall heat flux q_w and species mass fraction $Y^w_{N_2}$ and Y^w_O at the wall. All values refer to cases in which the DNS profile of the chemical reaction rate has been enforced in the solution, $\overline{\dot{w}}_i = f(y)|_{DNS}$. Errors are reported for both extended EWM and GFM at matching location $y^+_m = 100$. DNS data from Williams *et al.* (2023).

4. Conclusions

This study presents an *a priori* assessment of the accuracy of the extension of the GFM proposed by Griffin *et al.* (2023) to compressible turbulent reacting wall-bounded flows, comparing it with the accuracy of the extended EWM proposed by Di Renzo & Urzay (2019). The variability in the composition of the mixture near the wall is predicted by taking into account differential diffusion and finite-rate chemistry. Both models have been tested for the first time using DNS data from a strongly reacting turbulent boundary layer (Williams *et al.* 2023), which provides an essential reference given the enhanced turbulence–chemistry interaction in place. The extended GFM shows improved results when predicting the Favre-averaged wall-normal profiles of inner-scaled velocity u^+, rescaled temperature $\tilde{T}/T_w$, and enthalpy $\tilde{h}/h_{ref}$. This is reflected in the smaller modeling errors of wall shear stress τ_w, wall heat flux q_w, and most abundant species mass fractions $\tilde{Y}_{N_2}$ and $\tilde{Y}_O$, which are all below 3%.

The prediction of wall-normal profiles of mass fractions is comparable in both models, showing deviations from DNS especially in the prediction of wall-normal gradients at the matching location. These features are attributed to the absence of turbulence–chemistry interaction modeling in the prediction of the chemical reaction term $\overline{\dot{w}}$, which overshadows the respective model's differences on the predictions of the mean temperature and velocity profiles. This is confirmed by enforcing the DNS profiles of $\overline{\dot{w}}$ to both models, which clearly improves the overall estimate of composition for the extended GFM.

Acknowledgments

M.C. is supported by the Franklin P. and Caroline M. Johnson Fellowship in the School of Engineering Fund at Stanford University, Fulbright Italy, Zegna Founder's Scholarship and Fondazione Cassa di Risparmio di Padova e Rovigo. C.T.W. acknowledges support by the National Science Foundation Graduate Research Fellowship Program under Grant No. DGE-2146755. K.P.G. is supported by the Exascale Computing Project (Grant17-SC-20SC). The authors thank Dr. Mario Di Renzo for his support on the computational framework and Dr. Donatella Passiatore for the critical review of this manuscript.

This work was authored in part by the National Renewable Energy Laboratory, operated by Alliance for Sustainable Energy, LLC, for the U.S. Department of Energy (DOE) under Contract No. DEAC3608GO28308. The views expressed in the article do not nec-

REFERENCES

Anderson, J. D. 2006 *Hypersonic and High-temperature Gas Dynamics*. American Institute of Aeronautics and Astronautics.

Bertin, J. J. & Cummings, R. M. 2006 Critical hypersonic aerothermodynamic phenomena. *Annu. Rev. Fluid Mech.* **38**, 129–157.

Bose, S. T. & Park, G. I. 2018 Wall-modeled large-eddy simulation for complex turbulent flows. *Annu. Rev. of Fluid Mech.* **50**, 535–561.

Candler, G. V. 2019 Rate effects in hypersonic flows. *Annu. Rev. Fluid Mech.* **51**, 379–402.

Cogo, M., Baù, U., Chinappi, M., Bernardini, M. & Picano, F. 2023 Assessment of heat transfer and Mach number effects on high-speed turbulent boundary layers. *J. of Fluid Mech.* **974**, A10.

Di Renzo, M., Fu, L. & Urzay, J. 2020 HTR solver: an open-source exascale-oriented task-based multi-GPU high-order code for hypersonic aerothermodynamics. *Comput. Phys. Commun.* **255**, 107262.

Di Renzo, M. & Urzay, J. 2019 An a priori study of the accuracy of an equilibrium wall model for dissociating air in supersonic channel flows. *Annual Research Briefs*, Center for Turbulence Research, Stanford University, pp. 29–40.

Di Renzo, M. & Urzay, J. 2021 Direct numerical simulation of a hypersonic transitional boundary layer at suborbital enthalpies. *J. Fluid Mech.* **912**, A29.

Duan, L. & Martin, M. 2011 Direct numerical simulation of hypersonic turbulent boundary layers. Part 4. Effect of high enthalpy. *J. Fluid Mech.* **684**, 25–59.

Griffin, K. P., Fu, L. & Moin, P. 2021 Velocity transformation for compressible wall-bounded turbulent flows with and without heat transfer. *P. Natl. Acad. Sci. USA* **118**.

Griffin, K. P., Fu, L. & Moin, P. 2023 Near-wall model for compressible turbulent boundary layers based on an inverse velocity transformation. *J. Fluid Mech.* **970**, A36.

Iyer, P. & Malik, M. R. 2019 Analysis of the equilibrium wall model for high-speed turbulent flows. *Phys. Rev. Fluids* **4**, 074604.

Kawai, S. & Larsson, J. 2010 A dynamic wall model for large-eddy simulation of high Reynolds number compressible flows. *Annual Research Briefs*, Center for Turbulence Research, Stanford University, pp. 5–37.

Larsson, J., Kawai, S., Bodart, J. & Bermejo-Moreno, I. 2016 Large eddy simulation with modeled wall-stress: recent progress and future directions. *Mech. Eng. Rev.* **3**, 15–00418.

Muto, D., Daimon, Y., Shimizu, T. & Negishi, H. 2019 An equilibrium wall model for reacting turbulent flows with heat transfer. *Int. J. Heat Mass Tran.* **141**, 1187–1195.

Park, C. 1990 *Nonequilibrium Hypersonic Aerothermodynamics*. Wiley.

Passiatore, D., Sciacovelli, L., Cinnella, P. & Pascazio, G. 2022 Thermochemical non-equilibrium effects in turbulent hypersonic boundary layers. *J. Fluid Mech.* **941**, A21.

Urzay, J. 2018 Supersonic combustion in air-breathing propulsion systems for hypersonic flight. *Annu. Rev. Fluid Mech.* **50**, 593–627.

Williams, C. T., Di Renzo, M. & Moin, P. 2023 Direct simulation of turbulence-chemistry interaction in a strongly reacting turbulent hypersonic boundary layer. *Annual Research Briefs*, Center for Turbulence Research, Stanford University, in press.

Yang, X. I. & Lv, Y. 2018 A semi-locally scaled eddy viscosity formulation for les wall models and flows at high speeds. *Theor. and Comput. Fluid Dyn.* **32**, 617–627.

Yang, X. I., Urzay, J., Bose, S. & Moin, P. 2018 Aerodynamic heating in wall-modeled large-eddy simulation of high-speed flows. *AIAA J.* **56**, 731–742.

Zhang, Y. S., Bi, W. T., Hussain, F. & She, Z. S. 2014 A generalized Reynolds analogy for compressible wall-bounded turbulent flows. *J. Fluid Mech.* **739**, 392–420.

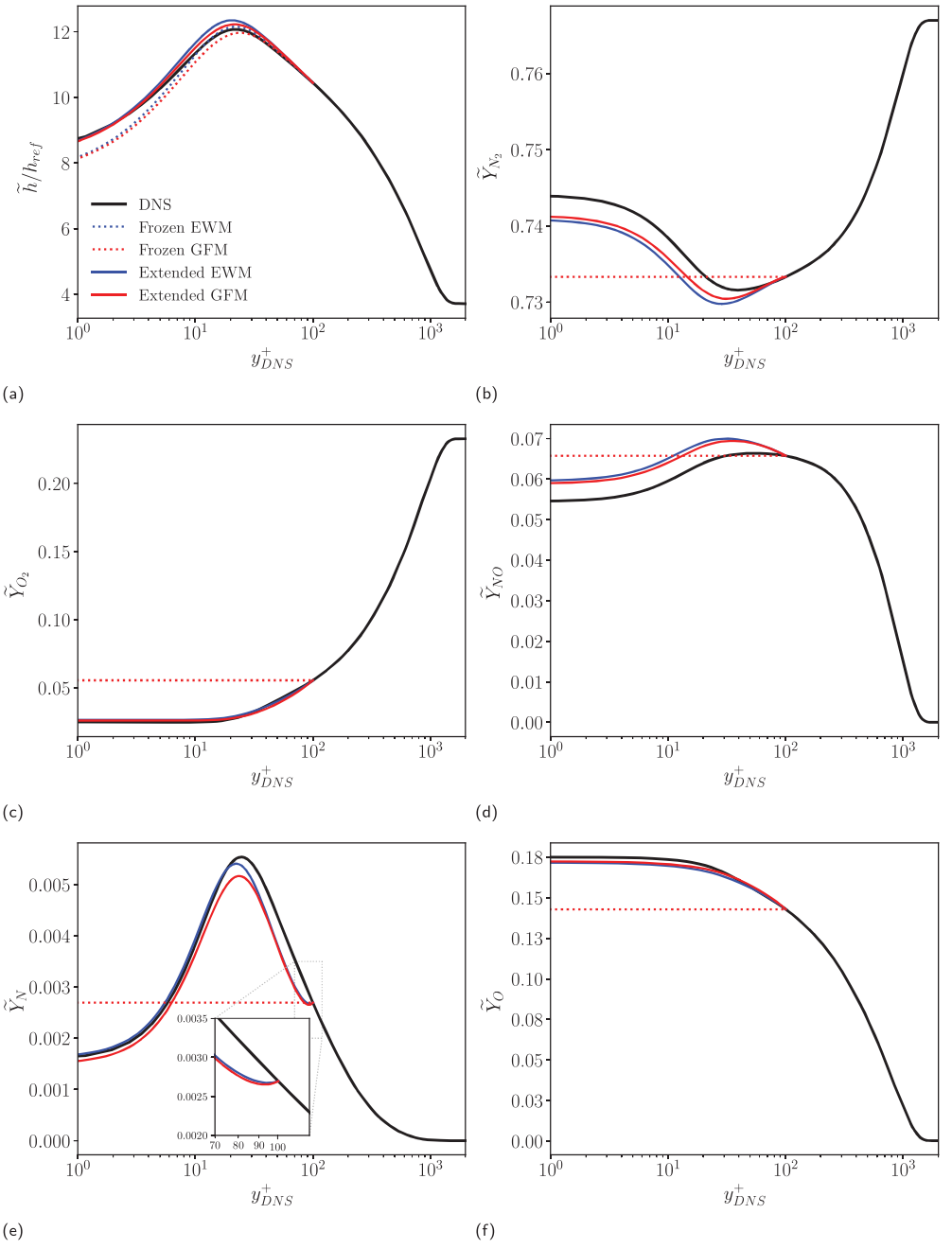

FIGURE 6. Favre-averaged profiles of (a) rescaled enthalpy $\tilde{h}/h_{ref}$ and (b-f) mass fractions $\tilde{Y}_{\mathrm{O}_2}$, $\tilde{Y}_{\mathrm{N}_2}$, $\tilde{Y}_{\mathrm{NO}}$, $\tilde{Y}_{\mathrm{N}}$, and $\tilde{Y}_{\mathrm{O}}$ as a function of y^+_{DNS}. The matching location corresponds to $y^+_{DNS} = 100$. DNS data from Williams *et al.* (2023).

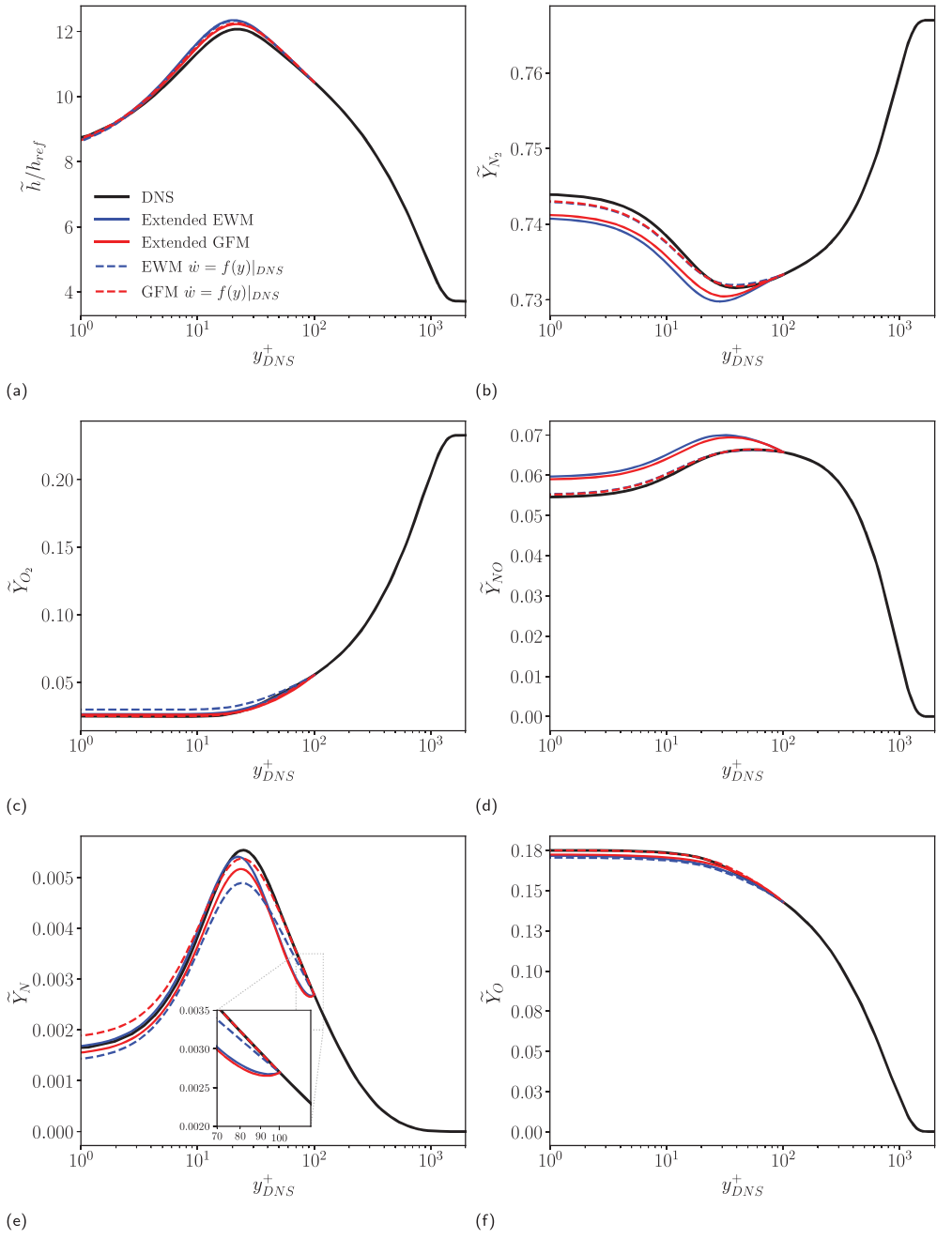

FIGURE 7. Favre-averaged profiles of (a) rescaled enthalpy $\tilde{h}/h_{ref}$ and (b-f) mass fractions $\tilde{Y}_{O_2}$, $\tilde{Y}_{N_2}$, $\tilde{Y}_{NO}$, $\tilde{Y}_N$, and $\tilde{Y}_O$ as a function of y^+_{DNS}. The matching location corresponds to $y^+_{DNS} = 100$. DNS data from Williams *et al.* (2023).